

# Reducing False Detection during Inspection of HDD using Super Resolution Image Processing and Deep Learning

Jirarat Ieamsaard<sup>1</sup>, Frode Eika Sandnes<sup>2,3</sup> and Paisarn Muneesawang<sup>1</sup>

<sup>1</sup>*Dept. of Electrical and Computer Eng., Faculty of Eng., Naresuan University, Phitsanulok, Thailand.*

<sup>2</sup>*Institute of Information Technology, Faculty of Technology, Art and Design, Oslo and Akershus University College of Applied Sciences, Oslo, Norway.*

<sup>3</sup>*Westerdals Oslo School of Art, Communication and Technology, Oslo, Norway.*  
*jirarati55@email.nu.ac.th*

**Abstract**—High false detection rates are a key reliability challenge in the Hard Disk Drive (HDD) industry. Therefore, automatic visual inspection is increasingly employed for HDD inspection. In order to improve the quality and reliability of HDD products, the false detection rate must be reduced. This paper presents a super-resolution image-based method for improving the performance of Head Gimbals Assembly (HGA) inspection. The experimental results confirm the efficiency of the super-resolution image processing for improving automatic inspection of defects such as pad burning and micro contaminations. Moreover, combining super resolution image processing with deep learning reduces the false detection rate and improves the accuracy of HGA inspection.

**Index Terms**—Image Super Resolution; HGA Inspection; Solder Ball Defect; Contamination Detection.

## I. INTRODUCTION

Automatic visual inspection systems are widely used in manufacturing industry to check the quality of products. False detection is a major concern in such inspection systems. In order to enhance the product quality and reliability, the accuracy and performance of the inspection systems must be improved such that the false detection rate is minimized.

In the Hard Disk Drive (HDDs) industry automatic visual inspection systems are applied in every step of the production line. However, there are several challenges due to the miniaturization of HDDs and their components. The key component responsible for the HDD read/write process is the head gimbals assembly (HGA). The HGA consists of two parts, namely the slider, which is the main part of the HGA consisting of a small circuit. The slider induces an electromagnetic field on the HGA, while reading and writing data from and to the disc platter. A HAG air bearing surface (ABS) moves above disc platter during the read/write process. Therefore, any contamination on the ABS causes reading and writing error. Next, the second part the suspension mechanism comprises flexure, a load beam and a base plate. Defects can occur if soldering mistakes happen while attaching the suspension mechanism during HGA slider assembly. If the defect occurs on the solder joint between the slider and the suspension mechanism, it may result in erroneous read/write processes.

This study proposes a method for improving the performance of the inspection systems for two of the most common HGA defects; the solder ball or pad burn and ABS

contamination defects. The inspections methods are improved by reducing the false detections caused by blurred images. The super-resolution image processing techniques are used to enhance the HGA image resolution.

## II. PREVIOUS WORKS

There are several studies that have addressed HDD inspection. [1] proposed a Bayesian-based method for inspecting HGA solder balls that achieved an accuracy of 91.52% with 660 blind test samples. [2] used fuzzy C-means clustering to classify HGA solder ball defect and achieved a high accuracy of 99.11% based on 225 test samples. [3] explored texture as a means for detecting ABS contamination. A study addressing solder ball inspection using VEDA and circular Hough transforms [4] yielded an accuracy of 99.32%. Contamination detection using likelihood approached and angle measurement has also been attempted<sup>5</sup> and this method is the basis for the work presented here in which improves the performance by including the super-resolution image technique.

## III. IMAGE SUPER RESOLUTION

Recently, deep convolution neural network (CNN) has been successfully applied to image super resolution. The super resolution method based on CNN proposed by [6,7] first, up scales input images using bicubic interpolation, then do patch extraction and representation, non-linear mapping, and finally reconstruction. Figure 1 shows the result of image super resolution; a) original blurred image without image super resolution, b) high resolution image after the image super-resolution process.

In this paper, we propose an adoption of the super-resolution convolutional neural network (SRCNN) [7]. The SRCNN has a simple structure with moderate numbers of filters and layers. This provides superior accuracy as well as less computation compared with state-of-the-art example based methods. This network has the fully feed-forward layers and does not need to solve any optimization problem. In addition, SRCNN processes the three channels of color images simultaneously to achieve improved super-resolution performance.

The detail of the three step super resolution method [7] is as follows: First, the input low-resolution image is up-scaled to the desired size using bicubic interpolation. Let the

interpolated image be denoted by  $\mathbf{Y}$ . Also, let  $F(\mathbf{Y})$  be the high resolution image which is recovered from  $\mathbf{Y}$ . The first step performs patch extraction and representation. The overlapped patches are extracted from the image  $\mathbf{Y}$  and represented by a high dimensional vector. Specifically, this is done by convolving the image by a set of filters in the first layer of the network:

$$F_1(\mathbf{Y}) = \max(0, W_1 * \mathbf{Y} + B_1) \quad (1)$$

where  $F_1$  is an operator,  $W_1$  and  $B_1$  represented the filters and biases respectively, and '\*' denotes the convolution operator. The first layer results in an  $n_1$ -dimensional feature vector for each patch.

In the second step, the second layer operation is applied to map the  $n_1$ -dimensional vectors to the  $n_2$ -dimensional vector. This operation is also based on convolution:

$$F_2(\mathbf{Y}) = \max(0, W_2 * F_1(\mathbf{Y}) + B_2) \quad (2)$$

where  $W_2$  and  $B_2$  are the filters and biases respectively. The  $n_2$ -dimensional vectors represented a high-resolution patch that will be used for reconstruction.

The last step reconstructs the high resolution image using an averaging filter:

$$F(\mathbf{Y}) = W_3 * F_2(\mathbf{Y}) + B_3 \quad (3)$$

Here,  $W_3$  corresponds to  $c$  filters and  $B_3$  is a  $c$ -dimensional vector.  $W_3$  is a set of linear filters, which obtains the average of the coefficients from the second layer.

The aforementioned operations lead to the same form as a convolution layer, and they can thus be implemented by a convolutional neural network.

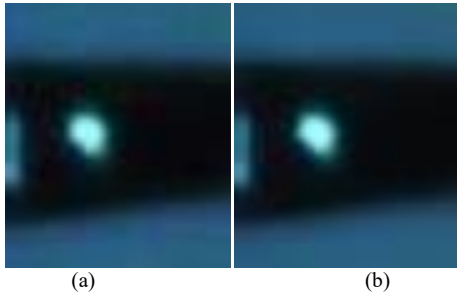


Figure 1: Image super-resolution example; a) original blurred image, and b) output of image super-resolution process.

#### IV. HGA INSPECTION

In the HGA production line, the HGAs are inspected by a machine comprising a camera module and a processing module. After transferring the HGA to the camera module, the HGA images are captured, then the HGA images are processed to detect HGA defects. The results are used by the module controller that controls all of machines in the production line. This section describes the inspection of defects in more detail.

##### A. Solder Defect Detection

The algorithm for solder ball or pad burnt detection is based on vertical edge detection and area-based analysis. First, the solder joint region is segmented from the original RGB HGA image with a dimension of  $2400 \times 2000$  pixels using cross correlation<sup>8</sup>. The solder joint template image, with a size of

$45 \times 420$  pixels, is used to find the reference point with the most corresponding points between the input image and the solder joint template image. From this reference point, we extracted a solder joint area with a size of  $45 \times 420$  pixels. Next, Otsu's method [4] is applied to convert solder joint RGB images into binary sub-images.

To detect vertical edges of solder balls or pads, Abbas M. Al-Ghaili et al.'s VEDA [9] algorithm is applied. The VEDA algorithm detects vertical edges based on moving a  $2 \times 4$  through the binary image to find intersections of black-white and white black pixels. By moving the  $2 \times 4$  mask, the vertical edges of solder joints or pad are detected as the black pixel, two- and one-pixel thick.

During the capturing of HGA images, there are often some reflections of light that occur within the pad. The circular vertical edges caused by the reflections may lead to erroneous decision making. Therefore, we apply the circular Hough transform [10] to identify the reflection areas.

The vertical edges of the reflections within the pads need to be removed in order to reduce the amount of erroneous decisions. We remove the vertical edges of the reflection areas by checking black pixels; all black pixels in the reflection area are set to white (background). For the burnt pad whose burnt area covers the entire pad from bottom to top, the VEDA output show that it has no vertical edge in the solder joint image. We identify this type of burnt pad using an area-based feature. We set the threshold of the pad area to 70% of the pad area noted as threshold T.

Finally, the decision-making process decides whether the test image is defective or not. First, we check the vertical edge image resulting from the VEDA algorithm, where black pixels indicate burnt objects. If the length of edge pixels is greater than edge threshold, set to 3 pixels, the test image is considered a defective image. Second, we check if the pad area is greater than the threshold T, in which case the test image is classified as defective image. Otherwise, the test image is considered a non-defective image. An example of circle detection by applying VEDA is shown in Figure 2.

To reduce the number of false detections caused by blurred images, image super-resolution is applied to the segmented solder region image before applying the edge detection and circle detection. False detections in non-defective images caused by blurring, as shown in Figure 3(a), can be reduced by image super-resolution as shown in Figure 3(b).

##### B. Detection of Contamination on ABS

To detect contaminations on the ABS, the  $490 \times 414$  pixel ABS region is segmented from a  $2400 \times 2000$  pixel HGA top view image using normalized cross-correlation [5]. The segmented ABS is registered with the ABS template using intensity-based registration [5]. Then, the grayscale ABS image is up-sampled 5 times in order to detect the very small contamination. A  $15 \times 15$  median filter is applied to anti-alias the image before detecting the potential area of contamination using the circular Hough transform. The circle parameter; circle center and radius are converted back to the coordinate system of the original size of the ABS image [5].

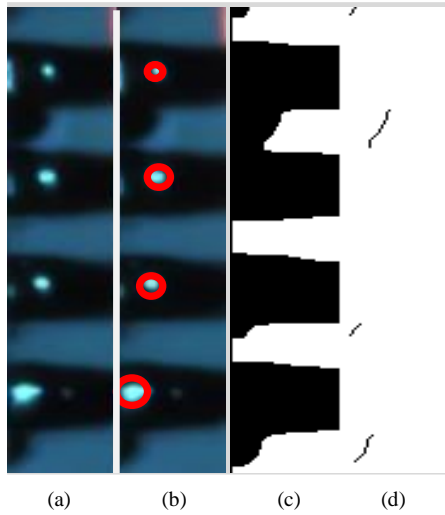


Figure 2: Solder ball or pad burnt detection; (a) solder region, (b) detect reflection using circular detection, (c) binary image, and (d) VEDA output

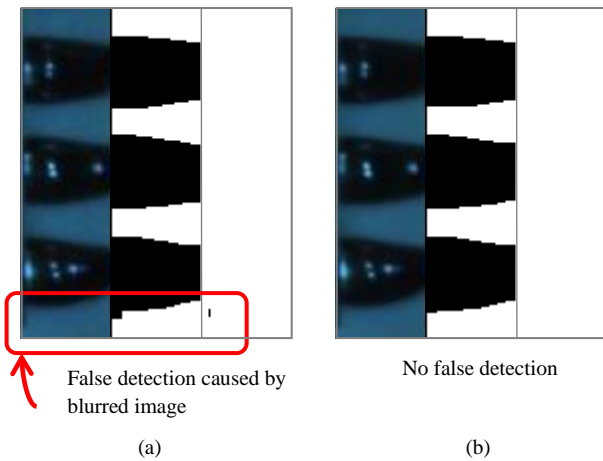


Figure 3: Example of image super-resolution; (a) resulting image without image super-resolution, and (b) resulting image with image super-resolution.

To classify the detected circles as a contamination or non-contamination, the detected circles are traced on a skeleton of an ABS template image with 50% larger radius to find points where the circumference of the detected circles crosses the skeleton. Each circle is considered according to three cases; case1 where the number of cross-points is 0, case2 where the number of cross-points is 1, and case3 where the number of cross-points  $\geq 2$ . For case3, the angle between the two cross-points and the circle center is calculated. If there are more than two cross-points, the largest angle is selected. Next, the cross-covariance feature [11] is applied to obtain a measure of similarity between square region of the grayscale test image and the grayscale of template image, where the square region is determined according to the circle center and radius [5].

The algorithm also used a likelihood function to detect contamination. In order to calculate the likelihood for each cross-point, cross covariance features were collected from 427 contamination circles and 23,721 non-contamination circles. The likelihood function for each case was calculated using a histogram.

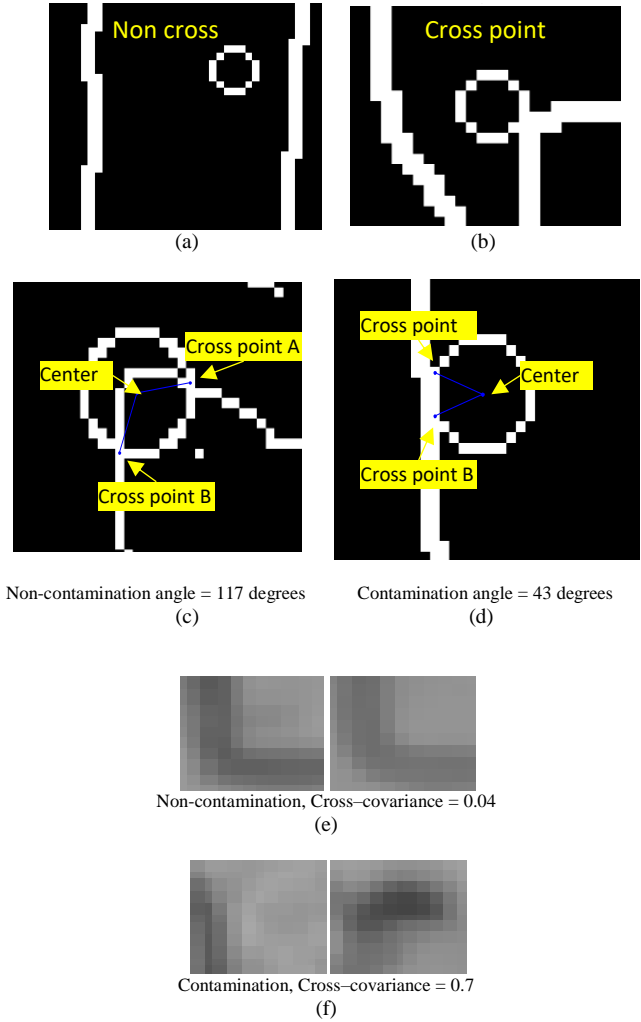


Figure 4: Contamination detection; (a) no cross-point, (b) no. cross-points =1, (c) no. cross-points  $\geq 2$  of Non-contamination circle, (d) no. cross-points  $\geq 2$  of contamination circle, (e) cross-covariance of non-contamination square, and (f) cross-covariance of contamination square.

For case 1 and case 2 the likelihood of each case is used to classify the detected circle into one of the two classes, namely the contamination class  $w_1$  or the non-contamination class  $w_2$ . From Bayesians theory one knows that  $P(w_i/x)$  varies directly with  $P(x/w_i)$ . If  $P(w_1/x)$  is greater than  $P(w_2/x)$ , the detected circle is considered contaminated. For case3, if the calculated angle is less than 90 degrees the circle area is considered contaminated. For circles with angles greater than 90 degrees, the likelihood is used to make a decision about whether the detected circle is contaminated or not [5].

In order to reduce the number of false inspections caused by blurred images, image super-resolution is applied to the tested image after ABS image segmentation. After the ABS image resolution is improved using image super resolution, false detection circles and cross-covariance error scores are reduced.

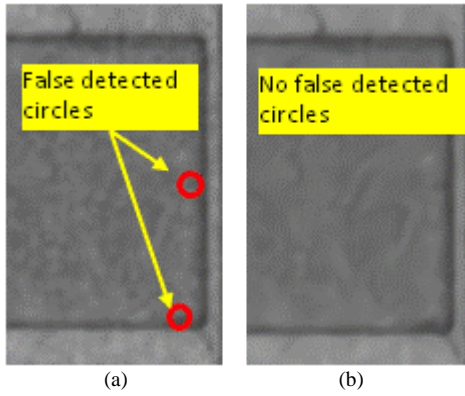


Figure 5: Example of circle detection with and without super resolution a) false detected circle in low resolution image, and b) no false detected circle in high resolution image.

V. EXPERIMENTAL RESULTS

The solder ball or pad burnt detection method is tested with 22,564 non-defective images and 1,089 defective images, where 100 images of non-defective images and 100 images of defective images were used in the training set to find the threshold value. The contamination detection algorithm is tested with 3,070 non-contamination images and 377 contamination images, where 1050 images of non-contamination images and 313 images of contamination images are used to calculate the likelihood function. The tested images and the trained images were captured by a mechanical positioning tool that positioned the camera while taking the pictures.

The performance of the defect and contamination detection of the method proposed herein were tested and compared to algorithms without image super-resolution.

False detections in non-contamination images and non-burnt defect on solder ball or pad images are denoted over-reject, and false detections in contamination images and solder ball or pad burnt images are denoted under-reject. The results of the solder ball or pad burnt detection are shown in Table 1. The result of the contamination detection is shown in Table 2. We also provide the result of the testing in term of accuracy using the training set in Table 3.

Table 1  
Experimental Results of Solder Ball or Pad Burnt Defect Detection

Over Reject	#samples	Non-Super resolution	%	Super resolution	%
1. Left_top	2379	7	0.29	5	0.21
2. Right_top	2490	11	0.44	8	0.32
Good_Left	3278	54	1.65	13	0.40
Good_Left2	3060	39	1.27	20	0.65
Good_Right	3001	37	1.23	24	0.80
Good_Right2	3356	43	1.28	9	0.27
Crop_Good	5000	64	1.28	33	0.66
Sum of over reject	22564	255	1.13	112	0.50
Under Reject					
J10_Image_Left	260	2	0.77	2	0.77
J10_Image_Right	299	4	1.34	2	0.67
J10_Crop	530	1	0.19	3	0.57
Sum of under reject	1089	7	0.64	7	0.64
Accuracy		98.89 %		99.50%	

The solder ball or pad burnt defect detection gave a high performance with an accuracy of 98.89%, 1.13% over-reject, and 0.64% under-reject. Using image super-resolution the accuracy is improved from 98.89% to 99.50%

The contamination detection method yields an accuracy of 81.58%, an over-reject rate of 17.07% and an under-reject rate of 29.44%. The contamination detection method including image super-resolution decreased the false detection both in terms of over-reject and under-reject, over-reject rate, under-reject rate, and accuracy, namely 16.78% and 20.42%, and 82.83% respectively.

Table 2  
Experimental Results of the ABS Contamination Detection

Test set	Non-super resolution %	Super resolution %
Over Reject (3,070 images)	524 17.07	515 16.78
Under Reject (377 images)	111 29.44	77 20.42
accuracy	81.58%	82.83 %

Table 3  
Test on Training Set

Test set	Percent of accuracy	
	Non-super resolution	Super resolution
Solder ball training set	99.30%	99.54%
ABS training set	81.78	99.14

VI. CONCLUSION

This paper presents a HGA inspection algorithm applying image super-resolution to reduce false detections caused by blurred images, where false detections are a concern during HGA inspections and need to be reduced in order to improve product quality. This paper focuses on solder ball or pad bunt defect detection and contamination detection. In solder ball burnt detection, over-rejects are reduced by 0.63%, which is small yet important improvement to the inspection system performance. The under reject rate of the ABS contamination detection is reduced by 9.02% which is a promising result. The experimental results validated the improvement gains achieved using image super-resolution. Future work includes improving the performance of the ABS contamination detection and reducing the false detection rate.

ACKNOWLEDGMENT

This project was financially supported by the Thailand Research Fund (TRF).

REFERENCES

- [1] C. W. Mak, N. V. Afzulpurkar, M. N. Dailey, and P. B. Saram, A Bayesian approach to automated optical inspection for solder jet ball joint defects in the Head Gimbal Assembly process, IEEE Trans. Automat. Sci. Eng., 11(4)(2014), 1155-1162.
- [2] R. Prasertaweelap, S. Kiatwanidvilai, Head Gimbal Assembly circuit with vision technique and Fuzzy C-Means Clustering. In Control, Automation and Systems (ICCAS) 15th International Conference on, (2015)October 13-16,177-180; Busan, Korea
- [3] P. Kunakornvong, C. Tangkongkiet, and P. Sooraksa, Defect detection on air bearing surface with luminance intensity invariance, in Proc. 9th Int. Conf. Fuzzy Syst. and Knowl. Discovery (FSKD), (2012) 693 – 696; China
- [4] J. Ieamsaard, S. Yammen, P. Muneesawang, F. E. Sandnes, Vertical dge detection-based automatic optical inspection of HGA solder jet ball joint defects, ECTI Transactions on Computer Eng, Computer and Information Technology, 9(2) (2015),173-181.
- [5] J. Ieamsaard, F. E. Sandnes, P. Muneesawang, Detection of micro contamination in hard disk drives using maximum likelihood estimation and angle detection, International Joint Conference on Computer Science and Software Engineering (JCSSE),

- (2016);Thailand.
- [6] C. Dong, C. C. Loy, K. He, X. Tang, Learning a deep convolutional network for image super-resolution. In *European Conference on Computer Vision*, Springer International Publishing. (2014) 184-199
- [7] C. Dong, C. C. Loy, K. He, X. Tang, Image super-resolution using deep convolutional networks. *IEEE transactions on pattern analysis and machine intelligence*, 38(2), (2016)295-307.
- [8] S. Yammen, and P. Muneesawang, An advanced vision system for the automatic inspection of corrosions on pole tips in hard disk drives, *IEEE Trans. Compon. Packag. Manuf. Technol.*, 4(9)(2014) 1523-1533
- [9] A. M. Al-Ghaili, S. Mashohor, A. R. Ramli, and A. Ismail, Vertical-edge-based car-license-plate detection method, *IEEE Trans. Veh. Technol.*, 62(1)(2013), 26-38
- [10] C. Chang, T. Chao, J. Horng, C. Lu, and R. Yeh, Development pattern recognition model for the classification of circuit probe wafer maps on semiconductors, *IEEE Trans. Compon. Packag. Manuf. Technol.*, 2(12)(2012), 2089-2097
- [11] P. Muneesawang, N. Zhang, and L. Guan, Image retrieval from a forensic cartridge case database, In *Multimedia Database Retrieval* Springer International Publishing, (2014)147-167.